with this, each representation of a rod and/or of a layer group engenders a certain representation of all those space groups which belong to corresponding layer and rod classes. This is a suitable regularity for systemization of representations (Kopský, 1988*b*). Accordingly, there also exists isomorphism of lattices of subgroups of subperiodic groups and of sublattices of 'partially equitranslational' subgroups in the lattices of subgroups of corresponding space groups (Kopský, 1987). This relationship is quite analogous to that between the lattices of subgroups of point groups and lattices of equitranslational subgroups of space groups as given by Ascher (1968).

Reducibility can also be introduced for the subperiodic groups themselves; this can be done for ordinary as well as for contracted subperiodic groups (Litvin & Kopský, 1987). As we can see, there are many viewpoints which have to be considered in connection with the extension of the reducibility concept to the Euclidean motion groups. Points 2 and 3 show the usefulness of the concept of reducibility and of the classification of space groups into subperiodic classes even on the level of groups up to three dimensions. Such a classification has been performed and will soon be published.

References

ASCHER, E. (1968). *Lattices of Equi-Translation Subgroups of the Space Groups.* Internal Report. Battelle Institute, Carouge, Switzerland.

ASCHER, E. & JANNER, A. (1965). *Helv. Phys. Acta*, **38**, 551-572.

ASCHER, E. & JANNER, A. (1968/69). *Commun. Math. Phys.* **11**, 138-167.

BOYLE, L. L. & LAWRENSON, J. E. (1973). *Acta Cryst.* A**29**, 353-357.

BROWN, H., BÜLOW, R., NEUBÜSER, J., WONDRATSCHEK, H. & ZASSENHAUS, H. (1978). *Crystallographic Groups of Four-Dimensional Space.* New York: Wiley.

COCHRAN, W. (1952). *Acta Cryst.* **5**, 630-633.

GIACOVAZZO, C. (1974). *Acta Cryst.* A**30**, 390-395.

HAHN, T. (1987). Editor. *International Tables for Crystallography.* Vol. A. Dordrecht: Reidel. (Present distributor Kluwer Academic Publishers, Dordrecht.)

HIRSHFELD, F. L. (1968). *Acta Cryst.* A**24**, 301-311.

JANOVEC, V., KOPSKÝ, V. & LITVIN, D. B. (1988). *Z. Kristallogr.* **185**, 282.

KOPSKÝ, V. (1987). *Czech. J. Phys.* B**37**, 785-808.

KOPSKÝ, V. (1988*a*). *Czech. J. Phys.* B**38**, 945-967.

KOPSKÝ, V. (1988*b*). *Int. J. Comput. Math.* **16**, 493-505.

KOPSKÝ, V. (1989). *Acta Cryst.* A**45**, 805-815.

KOPSKÝ, V. (1990). *Czech. J. Phys.* In the press.

LITVIN, D. B. & KOPSKÝ, V. (1987). *J. Phys. A: Math. Nucl. Gen.* **20**, 1655-1659.

MAXWELL, G. (1975). *J. Algebra*, **35**, 159-177.

SCHWARZENBERGER, R. L. E. (1980). *N-Dimensional Crystallography.* San Francisco: Pitman.

Acta Cryst. (1989). A**45**, 823-833

Theoretical Considerations on Two-Beam and Multi-Beam Grazing-Incidence X-ray Diffraction: Nonabsorbing Cases

BY HSUEH-HSING HUNG AND SHIH-LIN CHANG

Department of Physics, National Tsing-Hua University, Hsin-chu, Taiwan 30043

(*Received* 24 *January* 1989; *accepted* 7 *July* 1989)

Abstract

Two-beam and symmetric three- and four-beam grazing-incidence X-ray diffraction (GIXD) by crystals without absorption are studied based on the dynamical theory of X-ray diffraction. For two-beam cases, a new geometrical scheme is given to reveal graphically the excitation of the dispersion surface. For symmetric three- and four-beam cases, the expressions for specularly reflected and forward diffracted intensities are derived analytically. Results from the numerical calculations for the diffracted intensities, the penetration depths, the coordinates of the dispersion surface and the mode excitations are also presented for two-, three- and four-beam GIXD.

1. Introduction

Grazing incidence of X-ray scattering (GIXS), suggested by Marra, Eisenberger & Cho (1979), has been used as an experimental technique for probing the structures of crystal surfaces and overlayer interfaces. Its applications have recently been reviewed in an article by Fuoss, Liang & Eisenberger (1989). Theoretically, Vineyard (1982) described GIXS with a distorted-wave approximation in the kinematical theory of X-ray diffraction. In terms of the ordinary dynamical theory of Ewald (1917) and Laue (1931), Afanas'ev & Melkonyan (1983) worked out a formulation for the dynamical diffraction of X-rays under specular reflection conditions (GIXD - grazing-incidence X-ray diffraction) and Aleksandrov, Afanas'ev & Stepanov (1984) extended this formalism to include the diffraction geometry of thin surface layers. Subsequently, the properties of wavefields constructed during specularly diffracted reflections have been discussed in more detail by Cowan (1985) and Sakata & Hashizume (1987). Meanwhile, a geometrical interpretation of GIXS based on a three-

0108-7673/89/120823-11$03.00

dimensional dispersion surface has been proposed by Hoche, Brümmer & Nieber (1986).

In this paper we briefly review the dynamical theory of GIXD and give a new interpretation of the geometry of GIXD in momentum space. The dynamical theory of X-ray diffraction is then extended to multi-beam GIXD. The expressions of the forward reflected and specularly diffracted intensities are derived, as examples, for symmetric three-beam and four-beam GIXD in germanium crystals. For simplicity, absorption is not considered in the derivation. The penetration depths, excitation of mode of propagation as well as the diffracted intensities as a function of the incident angular position are also presented.

2. Dynamical theory of two-beam GIXD

(*A*) *Brief review of the theoretical background*

In an ordinary Bragg diffraction, there are two reciprocal-lattice points, say O and H, on the surface of an Ewald sphere. O and H represent the direct (incident) and the H-reflected beams, respectively. This is known as two-beam diffraction. When the angle of incidence is set in the vicinity of the critical angle of external total reflection (grazing incidence), more than two diffracted/reflected beams are generated because of the surface specular reflection. Fig. 1 is a schematic of grazing-incidence X-ray diffraction. For simplicity, we consider here only the σ-polarized incident X-ray E_0, perpendicular to the plane of incidence, in an ideally perfect crystal of infinite thickness. Under the conditions of specular reflection, the incident grazing angle φ is small, *i.e.* $\varphi \sim |\chi_0|^{1/2} \ll 1$, where $\chi_0/4\pi$ is the electric susceptibility of the direct reflection. The internal Bloch waves D_0 and D_h generated by diffraction are reflected from the crystal surface to give the specularly reflected and diffracted wavefields E_0^S and E_h^S. $\mathbf{k}$, $\mathbf{K}_0$, $\mathbf{K}_h$, $\mathbf{k}_0$ and $\mathbf{k}_h$ are the wavevectors of $\mathbf{E}_0$, $\mathbf{D}_0$, $\mathbf{D}_h$, $\mathbf{E}_0^S$ and $\mathbf{E}_h^S$, respectively. φ_h is the angle between $\mathbf{k}_h$ and the crystal surface. $\mathbf{H}$ is the reciprocal-lattice vector of the H reflection. ψ is the misorientation angle between the H planes and the crystal surface normal. $\psi \neq 0$ is referred to as an inclined geometric scheme. Although there are several reflected and diffracted beams generated for GIXD, only two reciprocal-lattice points are involved. We denote here this GIXD as a 'two-beam' case. Hereafter, N-beam GIXD will be used to denote the diffraction in which N reciprocal-lattice points are involved.

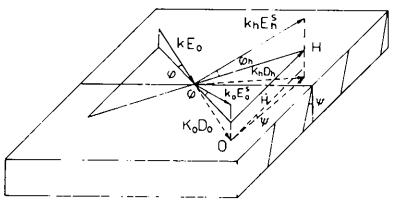

Fig. 1. Beam geometry of GIXD in real space.

The dynamical theory of two-beam GIXD has been formulated by Afanas'ev & Melkonyan (1983) within the framework of the Ewald–Laue theories. In order to provide a theoretical background for further derivation of multi-beam GIXD, we summarize the two-beam theory as follows:

For surface specular reflections, φ and ψ are very small, *i.e.* $\varphi, \psi \ll 1$. Under this condition, the angle of the specularly diffracted reflection φ_h can be expressed as

$$\varphi_h = (\varphi + \beta)^2 - \alpha_h, \tag{1}$$

where α_h is the angular deviation from the exact Bragg angle θ_B and β is the effective misorientation angle. Thus

$$\alpha_h = [(\mathbf{k}+\mathbf{H})^2 - k^2]/k^2 \tag{2}$$

$$\beta = 2\psi \sin\theta_B. \tag{3}$$

k, equal to $1/\lambda$, is the modulus of the wavevector in vacuum, λ being the wavelength of the X-ray used.

As is usual, the diffraction of X-rays from a crystal is described by the fundamental equation of wavefields. By solving this equation as an eigenvalue problem and employing the boundary conditions, the expressions for the wavefield amplitudes and the reflected intensities can be derived.

When the conditions $\psi = 0$ (symmetric geometry), $\alpha_h = 0$ (at the exact Bragg diffraction position) and $\chi_h = \chi_{\bar{h}}$ (nonabsorbing centrosymmetric crystals) are fulfilled, the following expressions are obtained for the absolute wavefield amplitudes:

$$D_0^{(1)} = -D_h^{(1)} = (\sin\varphi/C_1)E_0 \tag{4a}$$

$$D_0^{(2)} = D_h^{(2)} = (\sin\varphi/C_2)E_0 \tag{4b}$$

$$\begin{aligned} E_0^S &= -E_0 + (D_0^{(1)} + D_0^{(2)}) \\ &= \{[\sin^2\varphi - (\sin^2\varphi - \sin^2\theta_1)^{1/2} \\ &\quad \times (\sin^2\varphi - \sin^2\theta_2)^{1/2}]/C_1C_2\}E_0, \end{aligned} \tag{5a}$$

$$E_h^S = D_h^{(1)} + D_h^{(2)} = -[(C_2 - C_1)\sin\varphi/C_1C_2]E_0, \tag{5b}$$

where the characteristic angles are defined as

$$\left.\begin{matrix}\sin\theta_1 \\ \sin\theta_2\end{matrix}\right\} = (|\chi_0| \mp |\chi_h|)^{1/2} \tag{6}$$

and

$$C_i = \sin\varphi + (\sin^2\varphi - \sin^2\theta_i)^{1/2}. \tag{7}$$

χ_h is equal to ΓF_h, where F_h is the structure factor of the H reflection and $\Gamma = -r_e\lambda^2/\pi V$. r_e is the classical radius of the electron and V is the volume of the crystal unit cell.

The normalized intensities of the specular reflections are then equal to

$$P_0^S(\varphi) = |E_0^S|^2/|E_0|^2 \quad (8)$$

$$P_h^S(\varphi) = (|E_h^S|^2/|E_0|^2)(\varphi_h/\varphi). \quad (9)$$

In Fig. 2, the $P_0^S(\varphi)$ and $P_h^S(\varphi)$ are plotted for Ge (000)(220) GIXD for $\lambda = 3{\cdot}463683$ Å. The critical angles θ_1 and θ_2 are 6·542 and 15·962 mrad, respectively. The corresponding normalized reflection intensities are $P_{000}^S(\theta_1) = 0{\cdot}1680$, $P_{000}^S(\theta_2) = 0{\cdot}2735$, $P_{220}^S(\theta_1) = 0{\cdot}8320$, and $P_{220}^S(\theta_2) = 0{\cdot}2275$. Note that $P_{000}^S(\varphi) + P_{220}^S(\varphi) = 1$ for $\varphi \le \theta_1$.

(*B*) *New geometrical interpretation of the two-beam dispersion surface*

Hoche, Brümmer & Nieber (1986) have given a geometrical interpretation of the two-beam GIXD in terms of the dispersion surface. Figs. 3(*a*) and (*b*), adapted from their paper, are the two sections of the dispersion surface perpendicular and parallel to the crystal surface. From equation (1) of their paper, the relations among the tie points A_1 and A_2, the Lorentz point L_0 and the Laue point L_a are $ML_a = k\cos\theta_B$, $ML_0 = nk\cos\theta_B$, $MA_1 = (n - \chi_h/2)k\cos\theta_B$, $MA_2 = (n + \chi_h/2)k\cos\theta_B$, with $n = 1 + \chi_0/2$. The distance A_1A_2 is equal to $|\chi_h|k\cos\theta_B$. This is different from the value

$$A_1A_2 = k|\chi_h|/\cos\theta_B \quad (10)$$

in the ordinary dynamical theory of X-ray diffraction in a bulk crystal.

To clarify this inconsistency, we consider the azimuthal rotation of the crystal around the reciprocal-lattice vector **H**. The relation between the incident angle φ and the azimuthal tilting angle γ (see Fig. 3*b*) is

$$\sin\varphi = \cos\theta_B \sin\gamma. \quad (11)$$

$\varphi = 0$ as $\gamma \to 0$. Assume that $\gamma = \gamma_1$ and $\gamma = \gamma_2$ as $\varphi \to \theta_1$ and $\varphi \to \theta_2$, respectively. From Fig. 4(*a*), a section of the dispersion surface of the ordinary two-beam diffraction near the Lorentz point, the distance PQ between the incident wavefront Σ_0 in vacuum and the wavefront Σ_0' in the crystal is $PQ = k\chi_0/2$. The geometrical relations among the points P, Q, the tie points A_1, A_2, the Lorentz point L_0 and the Laue point L_a are

$$A_1Q = k\chi_h/2, \quad A_1L_a = k(\chi_0 - \chi_h)/(2\cos\theta_B),$$
$$L_0L_a = k\chi_0/(2\cos\theta_B). \quad (12)$$

The projection of Fig. 4(*a*) onto the plane perpendicular to the crystal surface is shown in Fig. 4(*b*). E is the entrance point on the incident wavefront whose wavevector satisfies Bragg's law: $\mathbf{k}_h = \mathbf{k}_0 + \mathbf{H}$. According to Figs. 4(*a*) and (*b*), the distance A_1A_2 has its usual value as

$$A_1A_2 = |MA_1 - MA_2| = k\chi_h/\cos\theta_B, \quad (13)$$

where the relations

$$\cos\gamma_1 = 1 - (\chi_0 - \chi_h)/(2\cos^2\theta_B)$$
$$\cos\gamma_2 = 1 - (\chi_0 + \chi_h)/(2\cos^2\theta_B) \quad (14)$$

have been employed in deriving (13). From (13) and

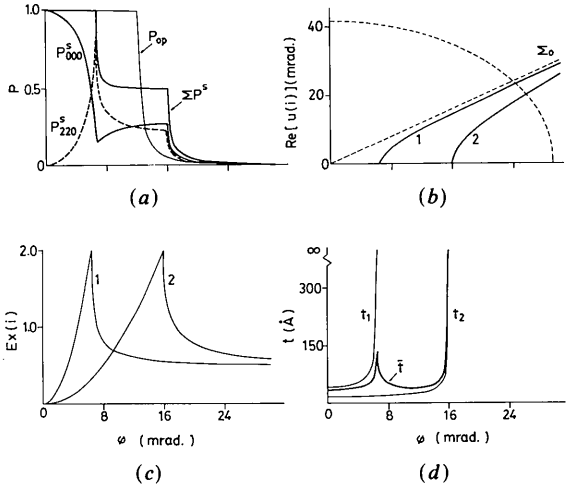

Fig. 2. Two-beam Ge (000) (220) GIXD for 3·463683 Å: (*a*) calculated intensities; (*b*) dispersion surface; (*c*) mode excitations; and (*d*) penetration depths.

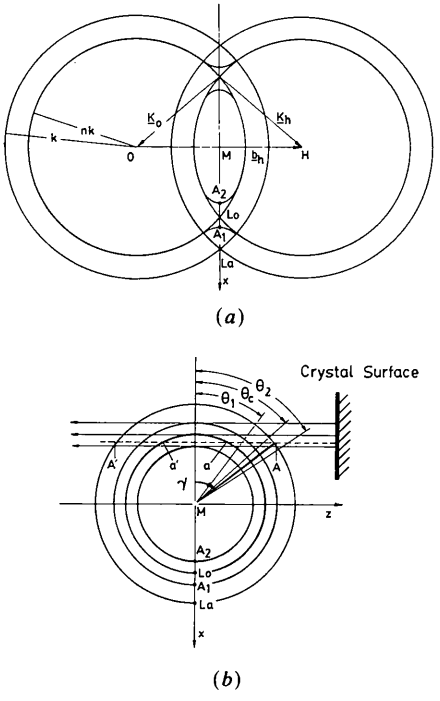

Fig. 3. (*a*) Section of the dispersion surface in the crystal surface; (*b*) section of the dispersion surface perpendicular to the crystal surface and bisecting the vector **OH**.

(14) and $\gamma_1, \gamma_2 \ll 1$, we arrive at the same expressions for θ_1 and θ_2, *i.e.* $\sin\theta_1 \simeq (|\chi_0 - \chi_h|)^{1/2}$ and $\sin\theta_2 \simeq (|\chi_0 + \chi_h|)^{1/2}$. The geometrical relations given in (13) should be consistent with the ordinary two-beam dynamical theory.

Moreover, the excitation of the dispersion surface with respect to the incident φ angle in two-beam GIXD can also be depicted geometrically in Fig. 4(*b*). Referring to Afanas'ev & Melkonyan (1983), we see that the dispersion equation can be written, in terms of the accommodation δ, normal to the crystal surface, as

$$\delta^2 - 2\delta\varphi = u^2 - \varphi^2, \tag{15}$$

or, more precisely,

$$\delta^2 - 2\delta \sin\varphi = \sin^2 u - \sin^2\varphi, \tag{16}$$

where u, a matching parameter of the wavevectors inside and outside the crystal at the crystal surface, is defined as

$$u = K_{0z}/k. \tag{17}$$

K_{0z} is the vector component of $\mathbf{K}_0$ perpendicular to the crystal surface. The permitted accommodation with $\mathrm{Im}(u) > 0$ is

$$\delta_i(\varphi) = \sin\varphi - \sin u^{(i)}, \tag{18}$$

where

$$\sin u^{(i)} = K_{0z}/k = (\sin^2\varphi - \sin^2\theta_i)^{1/2} \sim (\varphi^2 - \theta_i^2)^{1/2}. \tag{19}$$

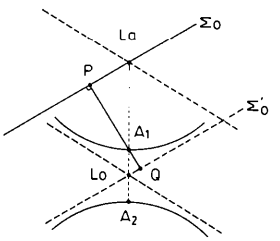

(*a*)

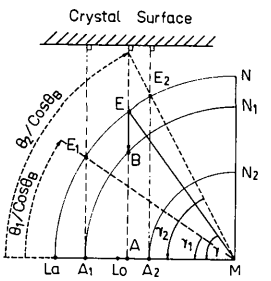

(*b*)

Fig. 4. (*a*) Section of the dispersion surface in the plane of incidence for a two-beam crystal diffraction; (*b*) geometrical representation for the excitation of the dispersion surface in two-beam GIXD.

$\mathrm{Im}(u)$ stands for the imaginary parts of u. The superscript and subscript i indicate the i mode. The angle θ can also be defined as

$$\cos\theta = K_0/k,$$

namely,

$$-2\varepsilon_0 = -(K_0^2 - k^2)/k^2 = \sin^2\theta.$$

By considering the cosine rule for the triangle BEM and the relation $AE = k\cos\theta_B \sin\gamma = k\sin\varphi \simeq k\varphi$, it can be shown that, for a given entrance point E,

$$\overline{BE} = k\delta, \quad \overline{AB} = ku. \tag{20}$$

This indicates that for $\theta_1 < \varphi < \theta_2$, the incident wave from the entrance point E excites the branch A_1N_1 of the dispersion surface at the point B. Since $\overline{BE}$ is perpendicular to the crystal surface, $\overline{BE}$ is therefore the resonance failure $k\delta_1$. The difference between AE and BE is then equal to the component K_{0z}. Since AE does not intersect the arc A_2N_2, $u^{(2)} = 0$, and so $k\delta_2 = k\varphi$. For $\varphi < \theta_1$, $u^{(1)} = u^{(2)} = 0$, $k\delta_1 = k\delta_2 = k\varphi$. For $\varphi > \theta_2$, AE always intersects with the arcs A_1N_1 and A_2N_2, say at B_1 and B_2. The resonance failures are $k\delta_1 = B_1E$ and $k\delta_2 = B_2E$. Clearly, those modes with $k\delta$ linearly proportional to φ are envanescent waves. Others are transmission waves.

3. Theoretical considerations on *N*-beam symmetric GIXD

Consider a general N-beam GIXD (O, H, G, Q), where the N reciprocal-lattice vectors lie in a plane parallel to the crystal surface ($\psi = 0$). For a nontrivial N-beam GIXD situation, the wavevectors involved are not exactly coplanar. It will be shown later that the wavevectors must be slightly off the crystal surface so that the surface reflected beams have appreciable intensities.

For simplicity, the following assumptions are made for N-beam GIXD: (i) no misorientation between the atomic planes and the crystal surface normal, $\psi = 0$; (ii) no absorption, *i.e.* $\chi_h = |\chi_h|$; (iii) for centrosymmetric crystals, $\chi_{\bar{h}} = \chi_h$; (iv) the crystal always satisfies Bragg's condition for the H reflection but is subject to an azimuthal tilting γ around the **H** vector, *i.e.* $\alpha_h = 0$, $\varphi_h = \varphi$, $2\varepsilon_h = (K_h^2 - k^2)/k^2 = 2\varepsilon_0$ and $\sin\varphi = \cos\theta_h \sin\gamma$.

In the following, symmetric three- and four-beam GIXD are considered separately.

(*A*) *Three-beam case*: Ge (000)(220)(202) *for* λ = 3·464 Å. Consider the three-beam case (O, H, G) of a germanium crystal with $O = (000)$, $H = (220)$, and $G = (202)$. The geometry in reciprocal space is shown in Fig. 5(*a*). C is the center of the triangle OHG. The point M is at the middle of the reciprocal-lattice vector **OH** of the H reflection. The semicircle E_1E_2 is the locus of the Laue points rotating around **OH**

of the two-beam H reflection, so that $EO = EH = k$, $ME = k\cos\theta_B$. The azimuthal angle of rotation around **OH** is $\gamma = \angle EMC$. **EP** is perpendicular to the plane OHG, parallel to the crystal surface. T is a tie point such that $ET = k\delta$. The wavevectors inside the crystal are $\mathbf{K}_0 = \mathbf{k}_0 + k\delta\hat{\mathbf{z}} = \mathbf{TO}$, $\mathbf{K}_h = \mathbf{k}_h + k\delta\hat{\mathbf{z}} = \mathbf{TH}$, and $\mathbf{K}_g = \mathbf{k}_0 + k\delta\mathbf{z} = \mathbf{TG}$. The angles of incidence and of reflection are $\varphi = \angle EOP$, $\varphi_h = \angle EHP$, and $\varphi_g = \angle NGP$, respectively. The arc NA is the wavefront of the G-reflected wave in vacuum. $\overline{E_3C}$ is normal to the crystal surface OHG and $E_3G = E_3O = E_3H = k$. E_3 is therefore the three-beam Laue point. The corresponding angles of incidence and azimuthal angle are $\varphi_3 = \angle E_3OC$ and $\gamma_3 = \angle E_3MC$, respectively. At point A, $\varphi_g = 0$. The corresponding azimuthal angle γ_A and incident angle φ_A can be calculated from the relations

$$\cos\gamma_A = 3\cos\gamma_3 - 1/\cos\theta_B \qquad (21a)$$

$$\sin\varphi_A = \cos\theta_B \sin\gamma_A. \qquad (21b)$$

From Fig. 5(a), the parameters u and v are defined as

$$\sin u = \sin\angle TOP = K_{0z}/K \qquad (22)$$

$$\sin v = \sin\angle TGP = K_{gz}/K. \qquad (23)$$

From the triangles E_3MO, CMO and E_3OC, the following relations are obtained:

$$\sin\theta_B \sin\angle ME_3O = \sin(\pi/3)\cos\varphi_3 \qquad (24)$$

$$\cos\gamma_3 = \tan\theta_B/\tan(\pi/3). \qquad (25)$$

The Bragg condition then takes the form

$$\lambda = 2d\sin(\pi/3)\cos\varphi_3, \qquad (26)$$

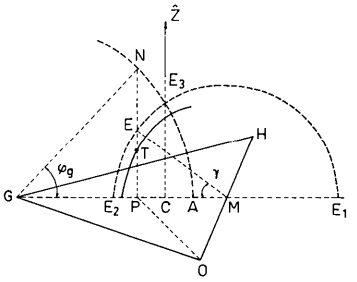

(a)

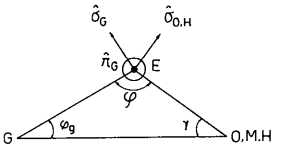

(b)

Fig. 5. (a) Schematic representation of a three-beam GIXD in reciprocal space; (b) definition of the polarization unit vectors of the three-beam case: $\hat{\boldsymbol{\pi}}_0$ and $\hat{\boldsymbol{\pi}}_H$ normal to $\hat{\boldsymbol{\sigma}}_0$ and $\hat{\boldsymbol{\sigma}}_H$ lie in the plane OEH.

where $\pi/3$ is the Bragg angle for a wavevector-coplanar symmetric three-beam GIXD. Equations (24) and (26) imply that for the non-coplanar three-beam diffraction, $\theta_B < \pi/3$ and $\lambda < 3{\cdot}46481$ Å. Since φ is in the range $0 \sim 50$ mrad, φ_3 can be chosen in the same angular range. Once φ_3 is fixed, the corresponding wavelength is then determined. Although φ_3 is small, the non-coplanar characteristics of the wavevectors introduce the correlation between σ- and π-polarized wavefields. This can be understood directly from the following fundamental equation of wavefields, where both σ and π polarization are considered:

$$\begin{bmatrix} \chi_0-2\varepsilon_0 & 0 & P_\sigma\chi_{\bar{h}} & 0 & d_2\chi_{\bar{g}} & 0 \\ 0 & \chi_0-2\varepsilon_0 & 0 & P_\pi\chi_{\bar{h}} & d_1\chi_{\bar{g}} & d_3\chi_{\bar{g}} \\ P_\sigma\chi_h & 0 & \chi_0-2\varepsilon_0 & 0 & d_2\chi_{h-g} & 0 \\ 0 & P_\pi\chi_h & 0 & \chi_0-2\varepsilon_0 & d_1'\chi_{h-g} & d_3'\chi_{h-g} \\ d_2\chi_g & d_1\chi_g & d_2\chi_{g-h} & d_1'\chi_{g-h} & \chi_0-2\varepsilon_g & 0 \\ 0 & d_3\chi_g & 0 & d_3'\chi_{g-h} & 0 & \chi_0-2\varepsilon_g \end{bmatrix} \begin{bmatrix} E_{\sigma 0} \\ E_{\pi 0} \\ E_{\sigma h} \\ E_{\pi h} \\ E_{\sigma g} \\ E_{\pi g} \end{bmatrix} = [0]. \qquad (27)$$

For simplicity, we assume $E_{\sigma 0} = E_0$ and $E_{\pi 0} = 0$. The polarization factors in (27) are

$$\begin{aligned} &P_\sigma = \hat{\boldsymbol{\sigma}}_0 \cdot \hat{\boldsymbol{\sigma}}_H = 1 \\ &P_\pi = \hat{\boldsymbol{\pi}}_0 \cdot \hat{\boldsymbol{\pi}}_H = \cos 2\theta_B \\ &d_1 = \hat{\boldsymbol{\pi}}_0 \cdot \hat{\boldsymbol{\sigma}}_G = \hat{\boldsymbol{\pi}}_H \cdot \hat{\boldsymbol{\sigma}}_G = d_1' = \sin(\pi-\varphi)\sin\theta_B \\ &d_2 = \hat{\boldsymbol{\sigma}}_0 \cdot \hat{\boldsymbol{\sigma}}_G = \hat{\boldsymbol{\sigma}}_H \boldsymbol{\sigma}_G = \cos(\pi-\varphi) \\ &d_3 = \hat{\boldsymbol{\pi}}_0 \cdot \hat{\boldsymbol{\pi}}_G = \hat{\boldsymbol{\pi}}_H \cdot \hat{\boldsymbol{\pi}}_G = d_3' = \cos 2\theta_B = P_\pi \\ &p(\text{others}) = 0. \end{aligned} \qquad (28)$$

The unit vectors $\hat{\boldsymbol{\sigma}}$'s and $\hat{\boldsymbol{\pi}}$'s are defined in Fig. 5(b), where $\varphi = \angle MEG$ and $\varphi_g' = \angle EGM$, and $\hat{\boldsymbol{\sigma}}_G$ and $\hat{\boldsymbol{\pi}}_G$ are perpendicular to $\mathbf{k}_g$ and EGM, respectively. Equation (27) can be written alternatively as

$$(\xi_0 + P_\sigma\chi_h)(\xi_0 + P_\pi\chi_h) \times \begin{vmatrix} \xi_h - P_\sigma\chi_h & -2d_2\chi_h & 0 & 0 \\ -2d_2\chi_h & 2\xi_g & -2d_1\chi_h & 0 \\ 0 & -2d_1\chi_h & \xi_h - P_\pi\chi_h & -2P_\pi\chi_h \\ 0 & 0 & -2P_\pi\chi_h & 2\xi_g \end{vmatrix} = 0, \qquad (29)$$

where $\xi_0 = -2\varepsilon_0 + \chi_0 = \xi_h$ and $\xi_g = -2\varepsilon_g + \chi_0 = \xi_0 - \alpha_g$. α_g is defined as

$$\alpha_g = (K_g^2 - K_0^2)/k^2 = -2\sin^2\theta_B(\cos\gamma/\cos\gamma_3 - 1). \qquad (30)$$

The relation still holds for three-beam GIXD:

$$\begin{aligned} -2\varepsilon_0 = \sin^2\theta &= \sin^2\varphi - (K_0/k)^2(K_{0z}/K_0)^2 \\ &= 2\delta\sin\varphi - \delta^2. \end{aligned} \qquad (31)$$

Thus,

$$\delta = \sin\varphi - (\sin^2\varphi - \sin^2\theta)^{1/2}. \qquad (32)$$

With the relations

$$n_0 = K_0/k = \cos\theta = \cos\varphi/\cos u \tag{33}$$

$$n_g = K_g/k = (1-\sin^2\theta+\alpha_g)^{1/2} = \cos\varphi_g/\cos v, \tag{34}$$

the α_g is simplified to

$$\alpha_g = \sin^2\varphi - \sin^2\varphi_g. \tag{35}$$

Since the polarization factor $d_1 = \sin(\varphi_g'+\gamma)\sin\theta_B \simeq (\varphi_g'+\gamma)\sin\theta_B$ is very small, it follows that (29) can be decomposed into two 3×3 matrix equations of the form

$$\begin{bmatrix} \xi_0 & P\chi_{\bar{h}} & P\chi_{\bar{g}} \\ P\chi_h & \xi_0 & P\chi_{h-g} \\ P\chi_g & P\chi_{g-h} & \xi_0-\alpha_g \end{bmatrix}\begin{bmatrix} E_0 \\ E_h \\ E_g \end{bmatrix} = 0, \tag{36}$$

where

$$P = \begin{cases} 1 & \text{for } \sigma \text{ polarization} \\ \cos 2\theta_B & \text{for } \pi \text{ polarization.} \end{cases}$$

The corresponding eigenvalues are

$$\text{mode 1 (or } H) \quad -2\varepsilon_0(1) = \sin^2\theta_1 = \chi_0 - \chi_h; \tag{37a}$$

$$\left.\begin{array}{ll} \text{mode 2 (or } -) & -2\varepsilon_0(2) = \sin^2\theta_2 \\ \text{mode 3 (or } +) & -2\varepsilon_0(3) = \sin^2\theta_3 \end{array}\right\} = \chi_0 + b_{\mp}\chi_h; \tag{37b}$$

where

$$b_{\mp} = [(1+\Delta_g) \mp (9-2\Delta_g+\Delta_g^2)^{1/2}]/2, \qquad \Delta_g = \alpha_g/\chi_h. \tag{38}$$

As α_g approaches zero, $\sin^2\theta_1 = (\chi_0-\chi_h)$ and $\sin^2\theta_2 = (\chi_0+2\chi_h)$. The eigenvectors are

$$\text{mode 1} \quad D_h(1) = D_0^{(1)}, \quad D_g(1) = 0; \tag{39a}$$

$$\text{mode 2} \quad D_h(2) = -D_0^{(2)}, \quad D_g(2) = 2^{1/2}\Delta_- D_0^{(2)}; \tag{39b}$$

$$\text{mode 3} \quad D_h(3) = -D_0^{(3)}, \quad D_g(3) = 2^{1/2}\Delta_+ D_0^{(3)}; \tag{39c}$$

where

$$\Delta_- = \Delta, \quad \Delta_+ = -1/\Delta, \tag{40}$$

$$\Delta = [\chi_h/2 - \alpha_g - (9\chi_h^2 - 2\alpha_g + \alpha_g^2)^{1/2}/2]/(2^{1/2}\chi_h). \tag{41}$$

As α_g approaches zero, $\Delta \to 2$.

The wavefield amplitudes inside the crystals are

$$D_0(1) = \tfrac{1}{2}(2\sin\varphi/C_1)E_0 \tag{42a}$$

$$D_0(2) = \tfrac{1}{2}a_-(2\sin\varphi/C_2)E_0 \tag{42b}$$

$$D_0(3) = \tfrac{1}{2}a_+(2\sin\varphi/C_3)E_0, \tag{42c}$$

where

$$1/a_- = 1+r, \quad 1/a_+ = 1+1/r \tag{43}$$

and

$$r = \Delta^2\left(\frac{C_3}{C_2}\right)\frac{\sin\varphi_g + (\sin^2\varphi - \sin^2\theta_2 + \alpha_g)^{1/2}}{\sin\varphi_g + (\sin^2\varphi - \sin^2\theta_3 + \alpha_g)^{1/2}}. \tag{44}$$

As φ approaches zero, $r \to 2$.

The specularly reflected wavefield amplitudes are

$$E_0^S = -E_0 + E_0(1/C_1 + a_-/C_2 + a_+/C_3)\sin\varphi \tag{45a}$$

$$E_h^S = E_0(1/C_1 - a_-/C_2 + a_+/C_3)\sin\varphi \tag{45b}$$

$$E_g^S = 2^{1/2}E_0(\Delta_- a_-/C_2 + \Delta_+ a_+/C_3)\sin\varphi. \tag{45c}$$

The corresponding reflection intensities are

$$P_0^S(\varphi) = |E_0^S|^2/|E_0|^2 \tag{46a}$$

$$P_h^S(\varphi) = |E_h^S|^2/|E_0|^2 \tag{46b}$$

$$P_g^S(\varphi) = (|E_g^S|^2/|E_0|^2)(\varphi_g/\varphi). \tag{46c}$$

For a wavevector-coplanar three-beam GIXD, $\varphi = \varphi_g = 0$ and $E_g^S = 0$. This trivial three-beam case with $P_g^S = 0$ is therefore physically not interesting.

(*B*) *Four-beam GIXD*: Ge (000)(220)(400)(2$\bar{2}$0) *for* $\lambda = 2{\cdot}828$ Å. Consider the four-beam (*O*, *H*, *G*, *Q*) case with $O = (000)$, $H = (220)$, $G = (400)$ and $Q = (2\bar{2}0)$. The four reciprocal-lattice points *O*, *H*, *G* and *Q* form a square. The Bragg condition for non-coplanar symmetric surface diffraction is

$$\lambda = 2d\sin(\pi/4)\cos\varphi_4, \tag{47}$$

where φ is the incident angle at which the four-beam GIXD takes place. From the diffraction geometry, the following useful relations are obtained:

$$\begin{aligned} &\sin\theta_B = \sin(\pi/4)\cos\varphi_4 \\ &\cos\gamma_4 = \tan\theta_B/\tan(\pi/4) \\ &\alpha_g = \alpha_q = -4\sin^2\theta_B(\cos\gamma/\cos\gamma_4 - 1) \\ &\cos\varphi_g = [\sin^2\theta_B + (2\sin\theta_B - \cos\theta_B\cos\gamma)^2]^{1/2} \\ &\cos\gamma_\Delta = 2\tan\theta_B - 1 \\ &\sin\varphi_\Delta = \cos\theta_B\sin\gamma_\Delta, \end{aligned} \tag{48}$$

where $\gamma \to \gamma_\Delta$, $\varphi \to \varphi_\Delta$ as $\varphi_g = 0$.

For simplicity, the small correlation between σ and π polarization for $\varphi \neq 0$ is ignored. The dispersion relation then takes the form

$$\begin{vmatrix} -\chi_0-2\varepsilon_0 & \chi_h & \chi_g & -\chi_h \\ \chi_h & -\chi_0-2\varepsilon_0 & -\chi_h & \chi_g \\ \chi_g & -\chi_h & -\chi_0-2\varepsilon_0-\alpha_g & \chi_h \\ -\chi_h & \chi_g & \chi_h & -\chi_0-2\varepsilon_0-\alpha_g \end{vmatrix} = 0, \tag{49}$$

where the phase relations $\chi_h = -\chi_q = -\chi_{h-g} = \chi_{g-q}$, $\chi_g = \chi_{h-g}$ ($\chi > 0$) have been used. Alternatively, (49)

can be written as

$$[(-2\varepsilon_0-\chi_0+\chi_h)(-2\varepsilon_0-\chi_0+\chi_h-\alpha_g)-(\chi_h-\chi_g)^2]\times[(-2\varepsilon_0-\chi_0-\chi_h)(-2\varepsilon_0-\chi_0-\chi_h-\alpha_g)-(\chi_h+\chi_g)^2]=0. \quad (50)$$

The eigenvalues are

mode 1 (or − −)

$$\sin\theta_1=(\chi_0-\chi_h+\{\alpha_g-[4(\chi_h-\chi_g)^2+\alpha_g^2]^{1/2}\}/2)^{1/2}; \quad (51a)$$

mode 2 (or −+)

$$\sin\theta_2=(\chi_0-\chi_h+\{\alpha_g+[4(\chi_h-\chi_g)^2+\alpha_g^2]^{1/2}\}/2)^{1/2}; \quad (51b)$$

mode 3 (or +−)

$$\sin\theta_3=(\chi_0+\chi_h+\{\alpha_g-[4(\chi_h+\chi_g)^2+\alpha_g^2]^{1/2}\}/2)^{1/2}; \quad (51c)$$

mode 4 (or ++)

$$\sin\theta_4=(\chi_0+\chi_h+\{\alpha_g+[4(\chi_h+\chi_g)^2+\alpha_g^2]^{1/2}\}/2)^{1/2}. \quad (51d)$$

As φ approaches zero,

$$\sin\theta_1\simeq|\chi_0-2\chi_h+\chi_g|^{1/2},\quad \sin\theta_2\simeq|\chi_0-\chi_g|^{1/2},\quad \sin\theta_3\simeq|\chi_0-\chi_g|^{1/2},\quad \sin\theta_4\simeq|\chi_0+2\chi_h+\chi_g|^{1/2}. \quad (52)$$

The eigenvectors are

mode 1 $D_h^{(1)}=D_0^{(1)}$,

$$D_g^{(1)}=D_g^{(1)}=\Delta_1 D_0^{(1)}=\Delta_- D_0^{(1)}; \quad (53a)$$

mode 2 $D_h^{(2)}=D_0^{(2)}$,

$$D_g^{(2)}=D_g^{(2)}=\Delta_2 D_0^{(2)}=-(1/\Delta_-)D_0^{(2)}; \quad (53b)$$

mode 3 $D_h^{(3)}=-D_0^{(3)}$,

$$D_g^{(3)}=-D_q^{(3)}=\Delta_3 D_0^{(3)}=\Delta_+ D_0^{(3)}; \quad (53c)$$

mode 4 $D_h^{(4)}=-D_0^{(4)}$,

$$D_g^{(4)}=-D_q^{(4)}=\Delta_4 D_0^{(4)}=-(1/\Delta_+)D_0^{(4)}; \quad (53d)$$

where

$$\Delta_-=\{\alpha_g-[4(\chi_h-\chi_g)^2+\alpha_g^2]^{1/2}\}/[2(\chi_h-\chi_g)], \quad (54a)$$

$$\Delta_+=-\{\alpha_g-[4(\chi_h+\chi_g)^2+\alpha_g^2]^{1/2}\}/[2(\chi_h+\chi_g)]. \quad (54b)$$

As φ approaches zero, $\Delta_-\simeq-1$ and $\Delta_+\simeq 1$.

The wavefield amplitudes inside the crystals are

$$D_0^{(1)}=\tfrac{1}{2}(2a_1\sin\varphi/C_1)E_0 \quad (55a)$$

$$D_0^{(2)}=\tfrac{1}{2}(2a_2\sin\varphi/C_2)E_0 \quad (55b)$$

Table 1. *Structure factors for germanium at room temperature*

λ (Å)	F_{000}	F'_{220}	F'_{400}
1·5406	245·6	173·4	142·9
2·8288	250·4	178·4	147·4
3·4644	250·4	178·4	147·4

The Debye parameter $B=0{\cdot}56$ Å is used for the structure-factor calculation.

$$D_0^{(3)}=\tfrac{1}{2}(2a_3\sin\varphi/C_3)E_0 \quad (55c)$$

$$D_0^{(4)}=\tfrac{1}{2}(2a_4\sin\varphi/C_4)E_0, \quad (55d)$$

where the C's have the same form as given in (7) and

$$1/a_1=1+r_-,\quad 1/a_2=1+1/r_-,\quad 1/a_3=1+r_+,\quad 1/a_4=1+1/r_+ \quad (56)$$

with

$$r_1=\Delta_-^2\left(\frac{C_2}{C_1}\right)\frac{\sin\varphi_g+(\sin^2\varphi-\sin^2\theta_1+\alpha_g)^{1/2}}{\sin\varphi_g+(\sin^2\varphi-\sin^2\theta_2+\alpha_g)^{1/2}}$$

$$r_2=\Delta_+^2\left(\frac{C_4}{C_3}\right)\frac{\sin\varphi_g+(\sin^2\varphi-\sin^2\theta_3+\alpha_g)^{1/2}}{\sin\varphi_g+(\sin^2\varphi-\sin^2\theta_4+\alpha_g)^{1/2}}. \quad (57)$$

The specularly reflected wavefield amplitudes are

$$E_0^S=-E_0+\left(\frac{a_1}{C_1}+\frac{a_2}{C_2}+\frac{a_3}{C_3}+\frac{a_4}{C_4}\right)E_0\sin\varphi \quad (58a)$$

$$E_h^S=\left(\frac{a_1}{C_1}+\frac{a_2}{C_2}-\frac{a_3}{C_3}-\frac{a_4}{C_4}\right)E_0\sin\varphi \quad (58b)$$

$$E_g^S=\left(\frac{\Delta_-a_1}{C_1}-\frac{a_2}{\Delta_-C_2}+\frac{\Delta_+a_3}{C_3}-\frac{a_4}{\Delta_+C_4}\right)E_0\sin\varphi \quad (58c)$$

$$E_q^S=\left(\frac{\Delta_-a_1}{C_1}-\frac{a_2}{\Delta_-C_2}-\frac{\Delta_+a_3}{C_3}+\frac{a_4}{\Delta_+C_4}\right)E_0\sin\varphi. \quad (58d)$$

The corresponding specularly reflected intensities are

$$P_0^S(\varphi)=|E_0^S|^2/|E_0|^2,\quad P_h^S(\varphi)=|E_h^S|^2/|E_0|^2,\quad P_g^S(\varphi)=(|E_g^S|^2/|E_0|^2)(\varphi_g/\varphi),\quad P_q^S(\varphi)=(|E_q^S|^2/|E_0|^2)(\varphi_q/\varphi). \quad (59)$$

4. Calculations

The calculation of specularly reflected intensities is based on the formulation derived in the previous section, with the structure factors at room temperature listed in Table 1 as the input data. The atomic form factors are taken from *International Tables for X-ray Crystallography* (1974) and extrapolated for $\lambda=2{\cdot}8288$ Å (four-beam case) and 3·4637 Å (three-beam case). The structure factors for the three-beam and the four-beam cases are given in Table 1. The temperature and anomalous-scattering effects are considered in the structure-factor calculation.

In Fig. 2(a), the curves of $\sum P^S$ ($=P_0^S+P_h^S$) and the optical reflection intensity P_{op} are also shown. The latter is calculated according to the Fresnel formula

$$P_{op}=\left|\frac{\sin\varphi-(n^2-\cos^2\varphi)^{1/2}}{\sin\varphi+(n^2-\cos^2\varphi)^{1/2}}\right|^2. \qquad (60)$$

For the two-beam (000), (220) of Ge and 3·463683 Å, the critical angle for P_{op} is $\theta_C=(|\chi_0|)^{1/2}=$ 12·198 mrad, which is between θ_1 (=6·5419 mrad) and θ_2 (=15·9616 mrad). The P_{000}^S curve first decreases in the range from $\varphi=0$ to $\varphi=\theta_1$, and then slightly increases for $\theta_1<\varphi<\theta_2$. For $\varphi>\theta_2$, P_{000}^S decreases monotonically. The reflection intensity P_{220}^S increases from zero to 0·83 at θ_1 and decreases monotonically for $\theta_1<\varphi<\theta_2$. P_{220}^S drops further for $\varphi>\theta_2$ and reaches zero intensity for $\varphi\gg\theta_2$. The $P_{000}^S+P_{220}^S$ curve shows that for $\varphi<\theta_1$, the total intensity is specularly reflected out of the crystal. For $\theta_1<\varphi<\theta_2$, half of the total intensity is transmitted into the interior of the crystal and half is specularly diffracted. For $\varphi<\theta_2$, most of the intensity is transmitted into the crystal. This explanation is consistent with the calculated penetration depths t_1 and t_2 for modes 1 and 2, and the resultant penetration depth $\bar{t}$ (Fig. 2d) which are defined as

$$t_i=1/[4\pi k\ \mathrm{Im}\,(\delta_i)] \qquad (61)$$

$$\bar{t}=\sum_{i=1,2} t_i\,\mathrm{Ex}\,(i), \qquad (62)$$

where the excitation Ex (i) of mode i is

$$\mathrm{Ex}\,(i)=\sum_{g=0,h} D_g^*(i)D_g(i)/|E_0|^2. \qquad (63)$$

In Fig. 2(d), t_1 and t_2 start with the values 42·1 and 17·3 Å at $\varphi=0$ and increase to infinity at $\varphi=\theta_1$ and $\varphi=\theta_2$, respectively. The resultant penetration depth $\bar{t}$ has an average value around 39 Å for $\varphi<\theta_2$ and has a peak value of 132 Å at $\varphi=\theta_1$. $\bar{t}$ reaches infinity at $\varphi=\theta_2$. Since absorption is not considered in the calculation, $\bar{t}$ is the average extinction length.

Fig. 2(b) shows the intersection of the dispersion surface with the plane of incidence. The abscissa is the scale for the incident angle φ. This horizontal axis also represents the crystal surface in real space. The ordinate stands for the quantity $u^{(i)}$ which indicates the position of a tie point measured upward from the crystal surface. The two curves are then the dispersion curves of mode 1 and mode 2 of propagation. The straight line across the figure diagonally represents the incident wavefront. The differences between this wavefront and the dispersion curves at a given φ are the δ values.

The excitations Ex (i) of the dispersion curves of modes 1 and 2 are shown in Fig. 2(c). Both modes behave similarly except that the maximum excitation, 200%, takes place at $\varphi=\theta_1$ for mode 1 and at $\varphi=\theta_2$ for mode 2. Ex (1) and Ex (2) approach asymptotically the value of 50% for $\varphi\gg\theta_2$, which is the one-beam (beam 000) excitation. The excitations exceeding 100% at $\varphi=\theta_1$ and $\varphi=\theta_2$ are due to the total reflection.

The calculated results for the three-beam case, Ge (000), (220), (202), for $\lambda=3{\cdot}463683$, 3·464341 and 3·464653 Å are shown in Figs. 6, 7 and 8, respectively. The three wavelengths correspond to the values of φ_3 chosen for the situations $\varphi_3<\theta_1$, $\theta_1<\varphi_3<\theta_2$, and $\theta_2<\varphi_3$, where $\theta_1\sim6{\cdot}5419$ and $\theta_2\sim15{\cdot}9616$ mrad. The three wavelengths, 3·463683, 3·464341 and 3·464653 Å, are calculated according to (26) for $\varphi_3=$ 24, 14 and 4 mrad, respectively. The corresponding φ_Δ are 29·393, 17·146 and 4·899 mrad.

The curves in Fig. 6(a) are the calculated P_{000}^S, P_{220}^S, P_{202}^S and $\sum P^S$ ($=P_{000}^S+P_{220}^S+P_{202}^S$) *versus* φ for $\lambda=3{\cdot}463683$ Å. Because φ_3 (=24 mrad) is far from θ_1 and θ_2, the presence of the 202 reflection has very little effect on P_{000}^S and P_{220}^S. Therefore, P_{000}^S, P_{220}^S and $\sum P^S$ behave like those in the two-beam case just discussed. P_{220}^S has an appreciable intensity about 0·056 near $\varphi=27{\cdot}75$ mrad. A small kink of 0·019 at $\varphi=16{\cdot}5$ mrad is observable.

There are three dispersion curves shown in Fig. 6(b). The curve of mode 1 is exactly the same as that in the two-beam case. This agrees with (37a). Curves 2 and 3 have the two-beam behavior of 220 and 202 reflections, respectively, as φ is far from φ_3 (=24 mrad). When φ approaches φ_3, modes 2 and 3 are dispersed from their two-beam curves, the dashed ones in Fig. 6(b). Resonance takes place at $\varphi=24{\cdot}50$ mrad, where the distance between curves 2 and 3 is minimal. Curves 1 and 2 cross over at φ_3. This means that modes 1 and 2 are degenerate. The wavefronts of the 000 and 202 diffracted waves are also denoted as Σ_0 and Σ_g in the same figure.

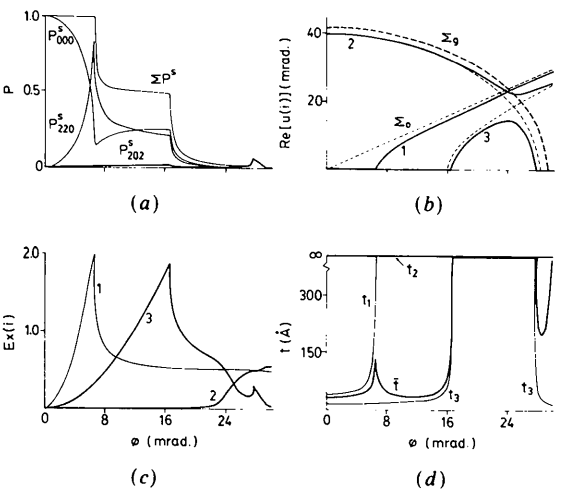

Fig. 6. Three-beam Ge (000), (220), (202) GIXD for 3·463683 Å: (a) calculated intensities; (b) dispersion surface; (c) mode excitations; (d) penetration depths.

The excitation Ex (1) of mode 1 is the same as in the two-beam case (see Fig. 6*c*). Ex (3) has a behavior similar to that of mode 2 in the two-beam case, except that near φ_3 the effect of the 202 reflection becomes appreciable. The small kink at $\varphi = 27{\cdot}75$ mrad is due to the total reflection occurring near the edge of the dispersion curve of mode 3 (see Fig. 6*b*). Ex (2) is almost zero for $\varphi < \varphi_3$. It increases near φ_3 and then reaches its two-beam value, 50%.

The penetration depths t_1, t_3 and the average depth $\bar{t}$ behave as the t_1, t_2 and $\bar{t}$ of the two-beam case for $\varphi < \theta_2$. For $\theta_2 < \varphi < 27{\cdot}75$ mrad, t_3 and $\bar{t}$ are infinite because of the total transmission of mode 3. As φ increases, t_3 decreases to the value of 17 Å, the two-beam depth. The average $\bar{t}$ has a minimum of 199 Å near 28·30 mrad. t_2 is always infinite. This total transmission seems to accompany the inward Poynting vectors normal to the dispersion curves of modes 1, 2 and 3.

Fig. 7 shows the calculated results for $\varphi_3 = 14$ mrad and $\lambda = 3{\cdot}464341$ Å. Because the two-beam dispersion curves (the dashed curves in Fig. 7*b*) of the 220 and 202 reflections do not intersect with each other, the dispersion curve of mode 3 is a line along the abscissa, in contrast to the hyperbola shown in Fig. 6(*b*) for $\lambda = 3{\cdot}463683$ Å. The surface-reflected intensities P^S_{000}, P^S_{220} and $\sum P^S$ therefore show no steps near θ_2. P^S_{202} increases from zero at $\varphi = 0$ and reaches a maximum due to the total reflection in the region ($\varphi \sim 15$ mrad) between the two dashed curves. P^S_{202} decreases abruptly at $\varphi \simeq 16{\cdot}5$ mrad (the point where Σ_g touches the crystal surface, namely $\varphi = 0$) and gradually tends to zero for large φ. The dispersion curves of modes 1 and 2 (Fig. 7*b*) are similar to those for $\lambda = 3{\cdot}463683$ Å shown in Fig. 6(*b*). The degeneracy takes place at φ_3 for modes 1 and 2.

The excitation of mode 1 remains unchanged (Fig. 7*c*). Ex (2) has a step at θ_2, while Ex (3) is almost a smooth curve with a maximum near φ_3. In Fig. 7(*d*), the penetration depths t_1, t_2 and $\bar{t}$ have similar behavior to those shown in Fig. 6(*d*) for $\lambda = 3{\cdot}463683$ Å, except that $\bar{t}$ does not have a minimum at $\varphi = 28$ mrad. t_3 shows a slowly varying curve, starting with 16·3 Å at $\varphi = 0$, reaching a maximum of 21·5 Å at φ_3, and decreasing towards 6 Å for large φ.

For $\varphi_3 = 4$ mrad and $\lambda = 3{\cdot}464653$ Å, the dispersion curves of modes 1 and 2 (see Fig. 8*b*) are similar to those in the two-beam case. The step of curve 2 occurs not at θ_2 (=15·96 mrad) but at $\varphi = 14{\cdot}5$ mrad. The dispersion curve of mode 3 is a straight line along the abscissa. Apparently, the wavefront Σ_g does not intersect with curves 1 and 2. Total reflection is expected to occur in the angular range from $\varphi = 0$ to $\varphi_\Delta \simeq$ 4·9 mrad (where Σ_g cuts the crystal surface). The P^S_{220} curve in Fig. 8(*a*) shows the total reflection intensities in the same range. The P^S_{000} shows accordingly a dip in this range. P^S_{220} and $\sum P^S$ resemble the two-beam curves of Fig. 2(*a*).

The excitation of mode 1, shown in Fig. 8(*c*), remains unchanged. The excitation of mode 2 resembles the two-beam curve, however, with a small kink feature at $\varphi_\Delta \simeq 4{\cdot}9$ mrad and a maximum of 2·2 at $\varphi = 14{\cdot}5$ mrad. The maximum value exceeding 200% in Ex (2) is due mainly to the definition of the excitation given in (63), where the directions of energy propagation are not considered. Mode 3 is excited in the range from 0 to 14·5 mrad, covering the total reflections of 202 and 220 reflections.

The penetration depth t_2 in the total reflection range decreases from 90·1 Å at $\varphi = 0$ towards the minimum value of 35 Å. t_1, t_3 and $\bar{t}$ behave similarly to those for $\lambda = 3{\cdot}464341$ Å shown in Fig. 7(*d*).

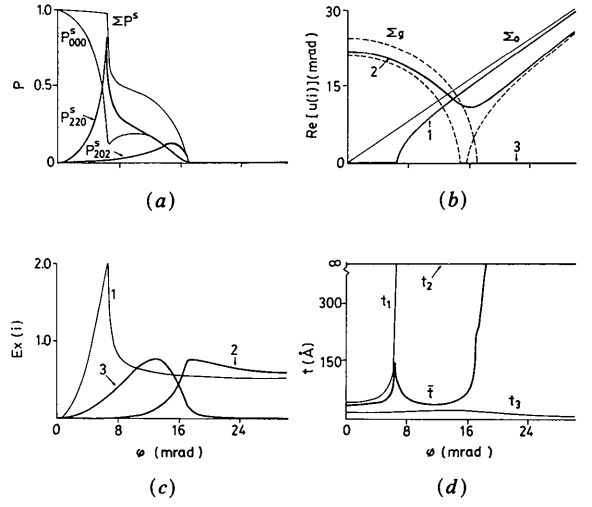

Fig. 7. Three-beam Ge (000), (220), (202) GIXD for 3·464341 Å: (*a*) calculated intensities; (*b*) dispersion surface; (*c*) mode excitations; (*d*) penetration depths.

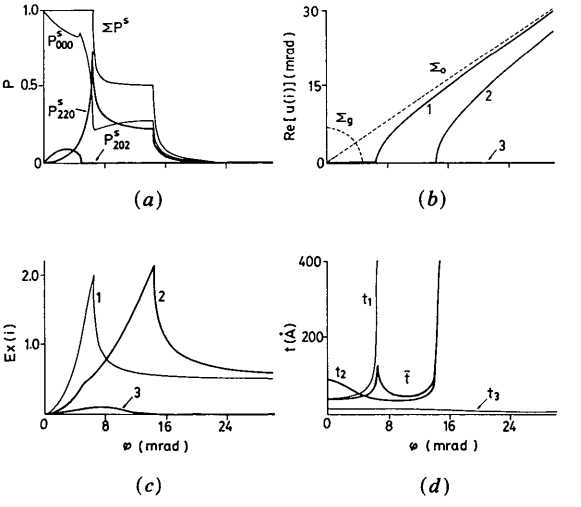

Fig. 8. Three-beam Ge (000), (220), (202) GIXD for 3·464653 Å: (*a*) calculated intensities; (*b*) dispersion surface; (*c*) mode excitations; (*d*) penetration depths.

Fig. 9 shows the calculated results for the four-beam GIXD Ge (000) (220) (400) ($2\bar{2}0$), where $\lambda = 2{\cdot}828696$ Å, $\theta_1 = 5{\cdot}3426$, $\theta_2 = 13{\cdot}0353$, $\theta_c = 9{\cdot}9614$, $\varphi_4 = 12$, and $\varphi_\Delta = 16{\cdot}9704$ mrad. In Fig. 9(a), the reflected intensities P^S_{000}, P^S_{220} and $\sum P^S$ resemble the intensity curves shown in Fig. 7(a). Maximum, minimum and steps take place at θ_1 for P^S_{000}, P^S_{220} and $\sum P^S$, respectively. P^S_{400} and $P^S_{2\bar{2}0}$ have relatively weak intensities. Maximal intensities at the exact four-beam position, φ_4, are 0·064 and 0·063 respectively for P^S_{400} and $P^S_{2\bar{2}0}$. At this position, P^S_{000} and P^S_{220} have also the same intensities as P^S_{400} and $P^S_{2\bar{2}0}$. All the intensities become null at $\varphi = \varphi_\Delta$.

The dispersion curves of modes 1, 2 and 3 follow asymptotically their two-beam dispersion curves Σ_g and Σ_2, respectively, for $\varphi < \varphi_4$ (Fig. 9b). Maximal dispersion occurs at φ_4. The dispersion curve of mode 4 is a straight line parallel to the crystal surface, with small and uniform penetration depths about 7–15 Å over the whole range of φ (see Fig. 9d). The excitations of mode 1 for $\varphi > \varphi_4$ and of mode 2 for $\varphi < \varphi_4$ exhibit the two-beam characteristics of the 220 reflection. Modification is found only near $\varphi = \varphi_4$. For $\varphi > \varphi_4$, a small kink taking place at $\varphi = 16{\cdot}25$ mrad is seen. This is due to the total reflection occurring at the edge of the dispersion curve 2. The excitation of mode 3 is a standard two-beam excitation with its maximum at θ_2. It decreases asymptotically to 50% for large φ. Mode 4, having an almost symmetric excitation, shows no special characteristics of wave interaction. At φ_4, modes 1, 2 and 3 have almost the same excitation. The transition from two-beam to four-beam and then to two-beam excitation is clearly shown: the two-beam (220 reflection) excitation of mode 2 dominates for $\varphi < \varphi_4$. It becomes four-beam excitation at φ_4. For $\varphi > \varphi_4$, the two-beam excitations of modes 1 and 3 are important.

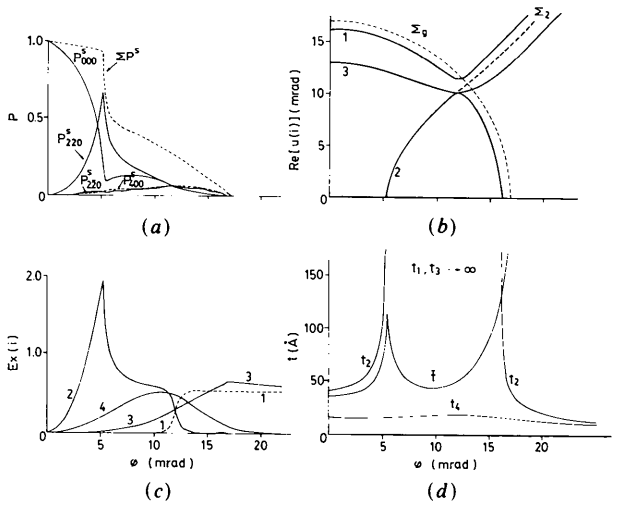

Fig. 9. Four-beam Ge (000), (220), (400), ($2\bar{2}0$) GIXD for 2·8288 Å: (a) calculated intensities; (b) dispersion surface; (c) mode excitations; (d) penetration depths.

Fig. 9(d) shows the penetration depth *versus* φ for this four-beam case. Modes 1 and 3, having infinite penetration depths, are totally transmitted through the crystal. Mode 2 has finite penetration depths in the total reflection ranges, *i.e.* $\varphi \lesssim \theta_1$ and $\varphi \gtrsim \theta_2$, and becomes total transmission in between. The average penetration depth therefore behaves very similarly to the two-beam case, where a maximum (of 114 Å) occurs at $\varphi = \theta_1$.

5. Discussion and concluding remarks

In the previous sections, we have dealt with three- and four-beam GIXD along the two-beam (say H) reflection line (*i.e.* the Bragg condition is always satisfied by the H reflection). From the geometry, it is clear that for $\varphi_N = 0$, with $N = 3$ and 4, the N-beam GIXD is a wavevector-coplanar multiple diffraction. The surface-reflected intensities of the reflections other than O and H are null. When $\varphi_N > 0$, the diffraction is no longer wavevector coplanar. Surface reflections with appreciable intensities are attainable. What has been discussed previously is therefore concerned with the situation in the vicinty of the exact N-beam GIXD. Because of the nature of grazing incidence for $\varphi_N > 0$, the dispersion surface lies above the crystal surface. This is clearly demonstrated in the calculations shown in Figs. 6, 7, 8 and 9.

Correlation between the σ- and π-polarized wavefields is another consequence of the non-coplanar diffraction. The order of magntidue of the π-polarized wavefields with respect to the σ-polarized ones can be estimated from the second row of (27). As $E_{\pi 0} = 0$ for a σ-polarized incident wave, the following relation holds:

$$d_1 \chi_{\bar{g}} E_{\sigma g} + P_\pi E_{\pi h} + d_3 \chi_{\bar{g}} E_{\pi g} = 0.$$

Thus

$$(E_{\pi h} + E_{\pi g})/E_{\sigma g} \sim \sin(\varphi'_g + \gamma) \sin\theta_B / \cos 2\theta_B \sim O(\varphi'_g + \gamma).$$

$O(\varphi'_g + \gamma)$ is about 0·05–0·001, which is so small that it can be neglected in the calculation. Errors due to this approximation are, however, readily detectable in the calculated curves $\sum P^S$ for $\varphi < \theta_1$ shown in Figs. 6(a) and 7(a), where $\sum P^S$ are supposed to be unity.

In the derivation and calculations given above, we have purposely ignored absorption so as to bring out the information about extinction, though the crystal and wavelength chosen heavily involve absorption. As can be seen from Figs. 2(d), 6(d), 7(d), 8(d) and 9(d), the average extinction lengths for these particular GIXD are around 15–50 Å. The maximum depths at the critical angle θ_1 are about 100–300 Å.

The phases about the structure factors involved, *i.e.* the signs for centrosymmetric crystals, are

necessary input for the calculation. According to (36) and (49), only the phase invariants of the structure-factor triplets and quartets affect the calculation.

Both the reflection intensities and mode excitations have peak values at the corresponding critical angles. This is due to the term $[\sin\varphi+(\sin^2\varphi-\sin^2\theta_i)^{1/2}]^{-1}$ involved in the wavefield amplitudes.

Small changes in φ_N cause large variations in the reflection intensities, as has already been shown in Figs. 6, 7 and 8. Experimentally, in order to detect this variation, strictly parallel and intense radiation sources with wavelength tunability are required. Use of synchrotron radiation is indispensable for carrying out the GIXD experiments (*e.g.* Cowan, Brennan, Jach, Bedzyk & Materlik, 1986; Sakata & Hashizume, 1988; Durbin & Gog, 1989).

In conclusion, we have derived analytical expressions for reflection intensity, wavefield amplitude and accommodation for two-beam and symmetric N-beam ($N>2$) GIXD. A new geometric scheme has also been provided in this study to reveal the excitation of the dispersion surface. Numerical calculation is straightforward for symmetric N-beam GIXD and should be modified for general asymmetric cases for which the obtaining of analytical expressions for intensities and wavefield amplitudes is not guaranteed.

The authors thank the National Science Council for financial support. One of the authors (HHH) is grateful to the same organization for providing a graduate fellowship.

References

AFANAS'EV, A. M. & MELKONYAN, M. K. (1983). *Acta Cryst.* A**39**, 207-210.
ALEKSANDROV, P. A'., AFANAS'EV, A. M. & STEPANOV, S. A. (1984). *Phys. Status Solidi A*, **86**, 143-154.
COWAN, P. L. (1985). *Phys. Rev. B*, **32**, 5437-5439.
COWAN, P. L., BRENNAN, S., JACH, T., BEDZYK, M. J. & MATERLIK, G. (1986). *Phys. Rev. Lett.* **57**, 2399-2402.
DURBIN, S. M. & GOG, T. (1989). *Acta Cryst.* A**45**, 132-141.
EWALD, P. P. (1917). *Ann. Phys. (Leipzig)*, **54**, 519-597.
FUOSS, P. H., LIANG, K. S. & EISENBERGER, P. (1989). In *Synchrotron Radiation Research: Advances in Surface Science*, edited by R. Z. BACHRACH. New York: Plenum.
HOCHE, H. R., BRUMMER, O. & NIEBER, J. (1986). *Acta Cryst.* A**42**, 585-587.
International Tables for X-ray Crystallography (1974). Vol. IV. Birmingham: Kynoch Press. (Present distributor Kluwer Academic Publishers, Dordrecht.)
LAUE, M. VON (1931). *Ergeb. Exakten Naturwiss.* **10**, 133-158.
MARRA, W. C., EISENBERGER, P. & CHO, A. Y. (1979). *J. Appl. Phys.* **50**, 6927-6933.
SAKATA, O. & HASHIZUME, H. (1987). Report RLEMTIT, **12**, 45-57. Research Laboratory of Engineering Materials, Tokyo Institute of Technology, Japan.
SAKATA, O. & HASHIZUME, H. (1988). *Jpn. J. Appl. Phys.* **27**, L1976-L1979.
VINEYARD, G. H. (1982). *Phys. Rev. B*, **26**, 4146-4159.

Acta Cryst. (1989). A**45**, 833-839

Determination of Crystal Structures from Poor-Quality Data Using Patterson Methods

BY C. C. WILSON

*Neutron Science Division, Rutherford Appleton Laboratory, Chilton, Didcot, Oxon OX*11 0*QX, England*

(*Received* 13 *March* 1989; *accepted* 19 *July* 1989)

Abstract

It is found to be possible to solve the structures of fairly simple materials from very poor-quality diffraction data by the use of reciprocal-space Patterson methods. Data sets assessed include those from a high-resolution neutron powder diffractometer, data sets with inaccurate randomized $|F_h|$ values, very small data sets (as few as ten reflections) and data sets with no estimates of $|F_h|$ values given. While refinement is not always feasible from such data it is found possible to obtain atomic positions and consequent structural information with reasonable accuracy. Reasons for using Patterson rather than direct methods in such cases are discussed.

Introduction

It is not always possible to collect good-quality structure-factor data from a crystallographic experiment. Problems can arise for various experimental reasons, owing, for example, to small poor-quality crystals, or to the existence of only a powder sample. The resolution of such experimental difficulties is beyond the scope of this work but rather the potential for the extraction of as much information as possible about the structure under such unfavourable circumstances will be discussed. It is in the area of garnering structural information from poor-quality data that Patterson methods have a significant advantage over direct methods, especially when the data are very scarce.

0108-7673/89/120833-07$03.00